Environmental Science & Technology

Article

Cite This: Environ. Sci. Technol. 2019, 53, 5797−5804

pubs.acs.org/est

Mechanism of Selective Ion Removal in Membrane Capacitive Deionization for Water Softening

Li Wang[†] and Shihong Lin*[,†,‡]

[†]Department of Civil and Environmental Engineering, Vanderbilt University, Nashville, Tennessee 37235-1831, United States

[‡]Department of Chemical and Biomolecular Engineering, Vanderbilt University, Nashville, Tennessee 37235-1604, United States

Supporting Information

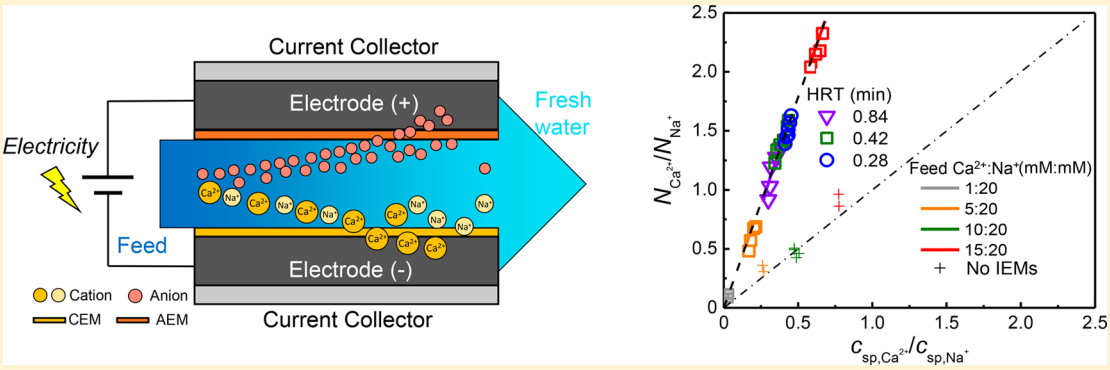

ABSTRACT: Capacitive deionization (CDI) is an emerging technology capable of selective removal of ions from water. While many studies have reported chemically tailored electrodes for selective ion removal, the selective removal of divalent cations (i.e., hardness) over monovalent cations can simply be achieved using membrane CDI (MCDI) equipped with ion exchange membranes (IEMs). In this study, we use both experimental and modeling approaches to systematically investigate the selective removal of Ca^{2+} over Na^{+}. Specifically, the impacts of current density, hydraulic retention time, and feed composition on the selectivity of Ca^{2+} over Na^{+} were investigated. The results from our study suggest a universal correlation between the ratio of molar fluxes and the ratio of spacer channel ion concentrations, regardless of operating conditions and feed composition. Our analysis also reveals inherent and universal trade-off relationships between selectivity and the Ca^{2+} removal rate and between selectivity and the degree of Ca^{2+} removal. This fundamental understanding of the mechanism of selective ion removal in MCDI can also be applied to flow-electrode CDI processes that employ IEMs.

INTRODUCTION

Hardness is a common water quality problem across the world, as ≥85% of the accessible fresh water is classified as hard water.[1] Water hardness in general can be attributed to multivalent cations and most often to calcium (Ca^{2+}) and magnesium (Mg^{2+}) that are typically abundant in groundwater. While hard water is generally not considered a health hazard, water of a high level of hardness undermines the efficacy of detergents[2] and promotes surface scaling[3] that is detrimental to water infrastructure and power plants. Hardness can be reduced by water softening using either chemical precipitation (i.e., lime-soda softening)[4,5] or ion exchange.[6−8] However, these processes either inherently require the use of chemicals or consume chemicals for regeneration. There is growing interest in chemical-free water treatment processes, especially in the context of decentralized small-scale water treatment. Therefore, other treatment technologies such as electrodialysis reversal[9−11] and nanofiltration[12−14] have been actively explored as an alternative process for water softening.

Capacitive deionization (CDI) is an emerging desalination technology that can potentially become a competitive, chemical-free technology for water softening.[15−17] In general, CDI works by removing the ions from the feed stream and temporarily storing the ions in the micropores of the electrode in the charging step and releasing those stored ions to the brine stream in the discharge step.[18,19] In theory, Ca^{2+} and Mg^{2+}, which have a valence of 2, should be preferentially removed by CDI over monovalent cations (e.g., Na^{+}) according to either the Guoy−Chapman−Stern (GCS)[20] or modified Donnan (mD) description of the equilibrium electrical double layer (EDL).[21] However, a previous study using CDI with constant-voltage charging revealed time-dependent ion selectivity, and consequently, the preferential removal of Ca^{2+} over Na^{+} can be achieved only when the charging step was prolonged far beyond the typical duration of a CDI charging step.[22]

To achieve selective Ca^{2+} removal within a typical charging step, it is possible to integrate ion exchange membranes

Received: January 30, 2019
Revised: April 11, 2019
Accepted: April 23, 2019
Published: April 23, 2019

DOI: 10.1021/acs.est.9b00655
Environ. Sci. Technol. 2019, 53, 5797−5804

(IEMs) to regulate the kinetics of ion transport. Specifically, if the use of a cation exchange membrane (CEM) favors the transport of divalent cations over monovalent cations,[23−25] then both electrostatic driving force and transport kinetics favor the accumulation of divalent cations over that of monovalent cations in the EDL, which may thereby result in water softening within a short duration typical of a half-operation cycle in CDI.

In a recent study, He et al. used flow-electrode CDI (FCDI) for brackish water softening.[26] The FCDI system showed significant selectivity of Ca^{2+} over Na^{+} in ion removal. The authors also reported the dependence of selectivity on current density and hydraulic retention time (HRT), which provides important insights regarding optimization of an FCDI-based water softening process. While FCDI differs from the more typical flow-by CDI processes in many aspects and has certain unique operational advantages,[27] we speculate that the Ca^{2+} selectivity observed in FCDI primarily stems from the use of a cation exchange membrane (CEM) that is an indispensable component of FCDI.[28−30] In water softening using ion exchange resins, the preferential removal of divalent cations over monovalent cations can be attributed to the stronger affinity of the ion exchange polymer for divalent cations as compared to that for monovalent cations.[23,25,31] This is also the primary reason why typical CEMs can promote faster preferential transport of divalent cations over monovalent cations and enable water softening in electrodialysis. For the same reason, membrane capacitive deionization (MCDI), i.e., CDI equipped with IEMs, should also have selectivity of divalent cations over monovalent cations due to the presence of CEMs (Figure 1).

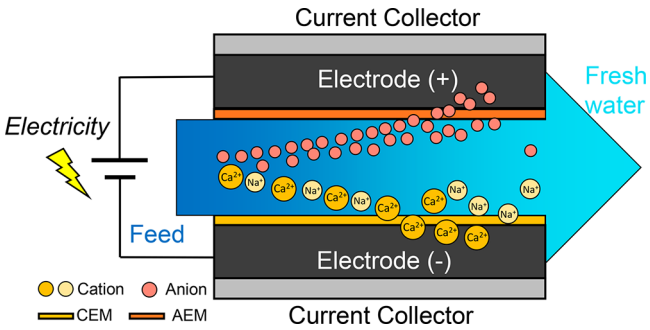

Figure 1. Schematic of water softening by an MCDI process. In this example with a feed solution containing two cations (Ca^{2+} and Na^{+}), Ca^{2+} is preferentially removed over Na^{+}.

While MCDI has been studied with a feed solution containing Ca^{2+},[16,32−36] surprisingly, only one very recent study has been performed to investigate the selective removal of ions from a feed solution of mixed cations using MCDI.[37] In this study, we perform both experiments and numerical simulations to systematically investigate selective ion removal by MCDI. Specifically, we develop a simple but effective model for describing the simultaneous transport of both divalent and monovalent cations in MCDI and use such a model to explain the results from a series of experiments performed using feed solutions containing both Ca^{2+} and Na^{+}. We present a universal correlation between the ion flux ratio and the ratio of spacer channel ion concentrations and apply that to explain the dependence of ion selectivity on three experimental parameters, including current density, HRT, and feed ion composition.

■ MATERIALS AND METHODS

MCDI Experimental Setup. All experiments were performed with a lab-scale MCDI module with four assemblies of electrodes, IEMs, and a spacer firmly pressed in an acrylic housing. Each assembly consists of two porous electrodes (PACMM 203, Materials & Methods LLC, Irvine, CA), a cation exchange membrane with a thickness (δ_{AMX}) of 140 μm, an anion exchange membrane with a thickness (δ_{CMX}) of 170 μm (Neosepta, Tokuyama Co.), and a glass fiber spacer with a thickness (δ_{sp}) of 250 μm (Whatman). Each assembly was cut to a 6 cm × 6 cm square with a 1.6 cm × 1.6 cm square hole in the center. The water entered the assembly from the periphery, flowed along the spacer channel, and exited through the center outlet. The total mass of the four pairs of electrodes was 3.06 g. Details about the MCDI stack layout are presented in Figure S1.

A peristaltic pump was used to drive the feed solution through the spacer channels in the MCDI stack. The feed solution was stored in a 10 L reservoir under constant nitrogen purging to minimize dissolved oxygen in the water. The effluent from the stack was continuously monitored with an in-line conductivity meter (isoPod EP 357, eDAQ) installed right at the exit of the module. The current was controlled by a potentiostat (SP 150, Bio-Logic), which also recorded the real-time voltage of the MCDI cell.

Experimental Design. The MCDI experiments were conducted with different hydraulic residence times (HRTs) and feed solutions with a series of Ca^{2+}/Na^{+} ratios. Because the available volume for solution in the MCDI stack was fixed, the HRT was controlled simply by adjusting the feed flow rate. In one series of experiments, three levels of HRT (0.28, 0.42, and 0.84 min) were tested while the feed composition was maintained as 10 mM $CaCl_2$ and 20 mM NaCl. In another series of experiments, the Ca^{2+}/Na^{+} ratio of the feed solution was systematically varied (1/20, 5/20, 10/20, and 15/20 mM) while the HRT was maintained as 0.42 min. The MCDI stack was charged at a constant current until the cell voltage reached a predefined cutoff voltage of 1.5 V. Because this study focuses on selective ion removal in the charging step, we simply apply zero voltage in the discharge step to complete the full charging/discharge cycle. To minimize the contribution of noncapacitive adsorption to ion removal, the feed solution was pumped through the MCDI stack until the effluent conductivity reached a stable level before the initiation of charging.

Because simple conductivity measurement cannot provide information regarding the effluent composition, effluent samples were collected for composition analysis. The collection of effluent samples started after at least three cycles to ensure that dynamic steady state (DSS) was achieved. The effluent from the MCDI stack was collected for the entire charging and discharge steps to measure the average concentrations. In several MCDI experiments that were also performed to validate the dynamic ion transport model, multiple effluent samples were collected at a fixed interval for the full charging/discharge cycle. The concentrations of Ca^{2+} and Na^{+} in the effluent samples were determined using inductively coupled plasma optical emission spectrometry (ICP-OES) (PerkinElmer Optima 8000DV). After each experiment, the MCDI system was rinsed with 1 mM HCl

DOI: 10.1021/acs.est.9b00655
Environ. Sci. Technol. 2019, 53, 5797−5804

and then doubly distilled water to remove any precipitate that may remain in the system. Three replicate experiments were performed for each condition, and the average concentration is reported with the standard deviation.

Performance Metrics for Selective Ion Removal. On the basis of a recent study by He et al.,[26] the selectivity of divalent cations Ca^{2+} over monovalent cations Na^+, $\rho(Ca^{2+}/Na^+)$, is defined as

$$\rho\left(\frac{Ca^{2+}}{Na^+}\right) = \frac{\Delta c_{Ca^{2+}}/c_{0,Ca^{2+}}}{\Delta c_{Na^+}/c_{0,Na^+}} \quad (1)$$

where $\Delta c_{Ca^{2+}}$ and Δc_{Na^+} are the decreases in Ca^{2+} and Na^+ concentrations in the charging step, respectively, and $c_{0,Ca^{2+}}$ and c_{0,Na^+} are the initial concentrations of Ca^{2+} and Na^+ in the feed stream, respectively. For each species i, the concentration reduction, Δc_i, is simply the difference between the feed concentration, $c_{0,i}$, and the average effluent concentration, $\overline{c}_{e,i}$:

$$\Delta c_i = c_{0,i} - \overline{c}_{e,i} \quad (2)$$

Another performance metric to be quantified is the average salt adsorption rate, ASAR, defined as the amount (mole or mass) of salt removed by a unit mass of electrode in a unit time, following eq 3

$$ASAR_i = Q\frac{\Delta c_i}{w_e} \quad (3)$$

where Q is the feed flow rate to the MCDI stack and w_e is the total mass of electrodes. We note that because this study focuses on the fundamental mechanism of selective ion removal, and $ASAR_i$ is defined for the charging step only instead of the entire charging/discharge cycle.

Selective Ion Transport Model. We employ a simplified zero-dimensional (0D) dynamic steady-state (DSS) model coupling the modified Donnan (mD) model and Nernst–Planck equation to describe dual cation transport. Most of the details are similar to those of the MCDI model with regard to the transport of a single cation species reported in our previous studies[38,39] and are thus described in detail only in the Supporting Information. Here, we highlight only several important equations pertinent to the model of transport of different cations through the cation exchange membrane (CEM), which is critical to the ion selectivity of the MCDI process.

In this 0D model, the spacer channel is assumed to be completely mixed and thus the ion concentration in the spacer channel is spatially uniform. Therefore, the bulk concentrations for species i used in selectivity analysis are simply the spacer channel concentrations, $c_{sp,i}$, which are also the effluent concentrations, $\overline{c}_{e,i}$. The concentration of ion i in the polymer CEM phase is related to that in the aqueous phase (i.e., spacer concentration, $c_{sp,i}$) by the partion coefficient K_i. Consequently, the relative molar flux between the Ca^{2+} and Na^+ in the CEM can be expressed as[25,40]

$$\left(\frac{N_{Ca^{2+}}}{N_{Na^+}}\right)_m = \frac{N_{m,Ca^{2+}}}{N_{m,Na^+}} = \frac{2D_{m,Ca^{2+}}K_{Ca^{2+}}}{D_{m,Na^+}K_{Na^+}}\frac{c_{sp,Ca^{2+}}}{c_{sp,Na^+}} \quad (4)$$

where $N_{m,Ca^{2+}}$ and N_{m,Na^+} are the molar fluxes of Ca^{2+} and Na^+ through the CEM, respectively, $c_{sp,Ca^{2+}}$ and c_{sp,Na^+} are the spacer channel concentrations of Ca^{2+} and Na^+, respectively, $D_{m,Ca^{2+}}$ and D_{m,Na^+} are the effective diffusion coefficients of Ca^{2+} and Na^+ in the CEM, respectively, and $K_{Ca^{2+}}$ and K_{Na^+} are the partion coefficients between the polymer phase and the aqueous phase (i.e., $K_i = c_{m,i}/c_{sp,i}$). The partition coefficients and effective diffusion coefficients are grouped together to become the transport selectivity factor, $P_{Na^+}^{Ca^{2+}}$:

$$P_{Na^+}^{Ca^{2+}} = \frac{2D_{m,Ca^{2+}}K_{Ca^{2+}}}{D_{m,Na^+}K_{Na^+}} \quad (5)$$

The transport selectivity factor relates the molar flux ratio of Ca^{2+} and Na^+ in the CEM to the spatial concentration ratio between Ca^{2+} and Na^+.

RESULTS AND DISCUSSION

Model Validation. Several cycles of cation adsorption and desorption were performed to validate the developed model and extract necessary parameters by fitting the effluent ion concentrations and cell voltage with respect to time. A typical CC-ZV MCDI cycle is presented in Figure 2 where empty symbols (Figure 2A) and dashed curves (Figure 2B) are the experimental data and solid curves are simulated results. For both Ca^{2+} and Na^+, the effluent concentration decreased to a steady-state concentration soon after the charging started. Even though the feed stream had a Na^+ concentration that was higher than the Ca^{2+} concentration, an additional decrease in the Ca^{2+} concentration was observed, which is indicative of selective removal of Ca^{2+} over Na^+. Specifically, the decreases in concentration for Ca^{2+} and Na^+ were 2.7 and 1.9 mM, respectively, even though the Na^+ concentration in the feed stream was twice the Ca^{2+} concentration. At the same time, the cell voltage increased virtually linearly over time until reaching the chosen cutoff voltage of 1.5 V. The electrodes were short-circuited in the ZV discharge step. The discharge was considered complete when the effluent concentrations of Ca^{2+} and Na^+ eventually became their respective influent concentrations.

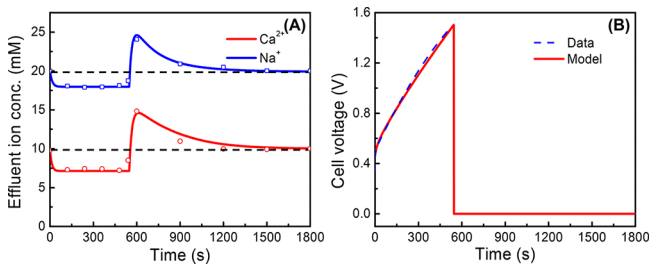

Figure 2. (A) Effluent concentrations of Ca^{2+} (red) and Na^+ (blue) in an MCDI process with CC-ZV operation. The empty symbols represent concentrations measured using ICP-OES, whereas the solid curves are simulated using the DSS MCDI model. (B) Cell voltage in an MCDI process with CC-ZV operation. The blue dashed curve represents data measured by the potentiostat, whereas the red solid curve is simulated using the DSS MCDI model. The feed solution contained 10 mM $CaCl_2$ and 20 mM NaCl. The flow rate was 8 mL min^{-1}, which corresponds to an HRT of 0.42 min. In the charging step, the current density was maintained at 7.48 A m^{-2} and the corresponding cell current was 100 mA. Charging was terminated when the cell voltage reached 1.5 V. The electrodes were short-circuited in the discharge step.

The simulated results from the DSS ion transport model fit the experimental results remarkably well (Figure 2). The good fitting suggests the validity of the DSS ion transport model in

DOI: 10.1021/acs.est.9b00655
Environ. Sci. Technol. 2019, 53, 5797−5804

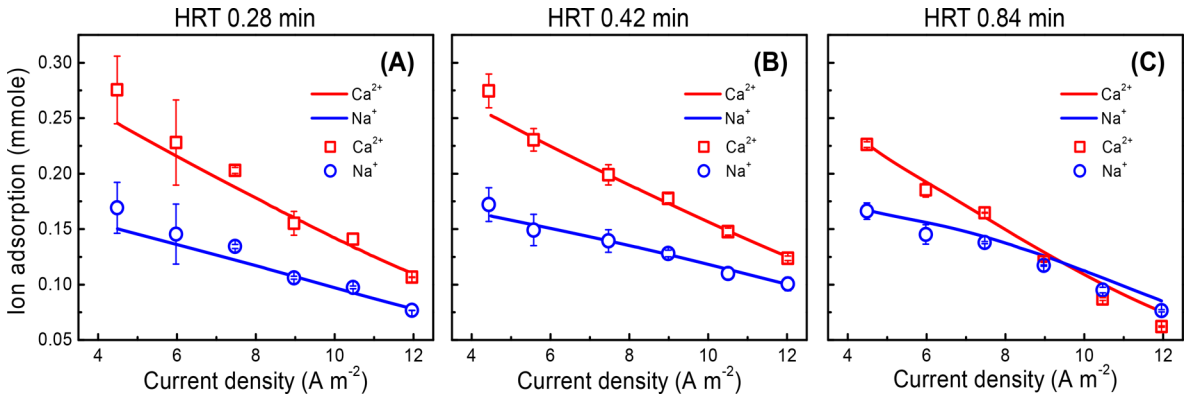

Figure 3. Ion adsorption as a function of current density at different HRTs: (A) 0.28, (B) 0.42, and (C) 0.84 min. The feed solution contained 10 mM $CaCl_2$ and 20 mM NaCl. The empty symbols are experimental data with the error bars representing standard deviations. The solid curves are generated from the DSS MCDI model and not from statistically fitting the experimental data.

describing the behavior of the MCDI stack. The parameters of the ion transport model, including those extracted from data fitting, are summarized in Table S1. This model will be used to elucidate the mechanism of selectivity and the dependence of selectivity on operating conditions in the following sections.

It has been reported in a previous study that the performance of MCDI with CC-ZV operation deteriorated almost immediately after the experiment started, especially when the cut voltage was high.[32] Specifically, it was observed that the initial charging voltage significantly increased in the first few cycles and the salt adsorption capacity (SAC) considerably decreased. The decline in the performance was attributed to the formation of the $Ca(OH)_2$ precipitate in the electrode. However, we did not observe such phenomena in our experiments. Both the initial charging voltage and the SAC were stable over multiple charging/discharge cycles (Supporting Information). There are several possible explanations for the different observations. As this is not the focus of this study, these explanations are detailed in the Supporting Information.

Selective Ion Removal. For the same feed stream, the removal of different cationic species strongly depends on the current density and HRT. For a given HRT, the total number of moles of ions removed decreases with an increase in current density (Figure 3). This is not surprising because a higher current density leads to faster ion transport and thus more ion removal in a given HRT. However, increasing the current density consistently reduced the selectivity, $\rho(Ca^{2+}/Na^{+})$, regardless of the HRT. Interestingly, changing the HRT does not seem to affect the removal of Na^{+} to any significant extent at a given current density. However, when the HRT was high, the adsorption of Ca^{2+} in the high-current density regime is significantly reduced (Figure 3C). With an HRT of 0.84 min and a current density beyond ~9 A m^{-2}, the adsorption of Ca^{2+} was reduced to an extent that the system no longer had preferential adsorption of Ca^{2+} over Na^{+}.

These observations can be explained by the fact that the degree of ion adsorption depends not only on current density, as Figure 3 clearly shows, but also on the spacer channel concentrations. For Na^{+}, the spacer channel concentration, $c_{sp,Na^{+}}$, did not change significantly as HRT increased. This is because even though $\Delta c_{Na^{+}}$ increased with a longer HRT, it was in all cases small compared to the feed concentration $c_{0,Na^{+}}$, which rendered the spacer channel concentration $c_{sp,Na^{+}}$ $(= c_{0,Ca^{2+}} - \Delta c_{Na^{+}})$ similar regardless of the HRT. However, because the feed stream concentration of Ca^{2+} was much lower at the start, a longer HRT, which led to a larger decrease in concentration, $\Delta c_{Ca^{2+}}$, resulted in a considerably lower $c_{sp,Ca^{2+}}$ $(=c_{0,Ca^{2+}} - \Delta c_{Ca^{2+}})$. With a long HRT and a high current density, $c_{sp,Ca^{2+}}$ became significantly reduced and the overall removal of Ca^{2+} was compromised to a great extent.

The argument presented above relating the overall ion removal to the spacer channel concentration also suggests that the feed composition should have a strong impact on the relative removal of Ca^{2+} and Na^{+}. Such an impact was also investigated using feed solutions with different Ca^{2+} concentrations and a fixed Na^{+} concentration of 20 mM. When the Ca^{2+} concentration was 1/20 of the Na^{+} concentration, the absolute amount of Ca^{2+} adsorbed was very small compared to the amount of Na^{+} (Figure 4A). The adsorption of Na^{+} was strongly dependent on current density, whereas the dependence of Ca^{2+} on current density was significantly weaker. Even in this case, however, the selectivity $\rho(Ca^{2+}/Na^{+})$ was still calculated to be from 1.60 to 2.43, meaning that Ca^{2+} was selectively removed over Na^{+}.

As $c_{0,Ca^{2+}}$ increased, the adsorption of Ca^{2+} was systematically enhanced (Figure 4B−D), which is unsurprising as the amount of Ca^{2+} adsorbed strongly depends on $c_{sp,Ca^{2+}}$, which in turn strongly depends on $c_{0,Ca^{2+}}$. Specifically, when $c_{0,Ca^{2+}}$ was 10 and 15 mM, the system removed more Ca^{2+} than Na^{+} even though the feed stream had more Na^{+} than Ca^{2+}, thanks to the selective removal of Ca^{2+} over Na^{+}. Another interesting observation is that the absolute level of Na^{+} adsorption was dampened with an increase in $c_{0,Ca^{2+}}$, especially in the low-current density regime. This may be explained by the competition of Ca^{2+} and Na^{+} for the limited adsorption capacity. While such an explanation may be valid, a more careful analysis suggests the adsorption capacity itself also increased with Ca^{2+} concentration. Specifically, the MCDI system removed more charges (i.e., $\Delta c_{Na^{+}} + 2\Delta c_{Ca^{2+}}$) from solutions with a feed solution with a higher Ca^{2+} concentration (Figure S1).

Mechanism of Selective Ion Removal with and without CEM. In the absence of CEM, the cation flux under a given electrical potential gradient should be proportional to the product of the ionic charge, the diffusion coefficient, and the concentration (i.e., $N_i \propto z_i D_i c_i$).[40,41] Unless the system reaches equilibrium as in the case of prolonged constant voltage charging, the competitive removal of Ca^{2+} and

DOI: 10.1021/acs.est.9b00655
Environ. Sci. Technol. 2019, 53, 5797−5804

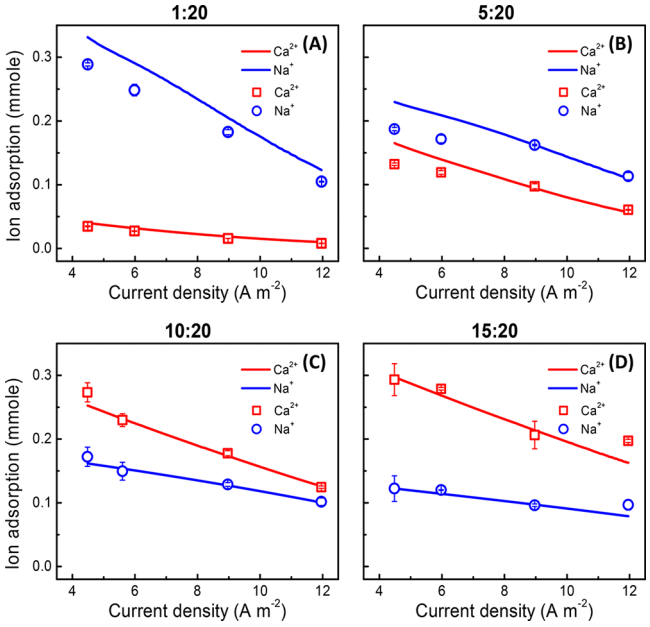

Figure 4. Ion adsorption as a function of current density for different feed compositions. The concentration of NaCl in the solution was 20 mM in all cases, whereas the concentrations of $CaCl_2$ were (A) 1, (B) 5, (C) 10, and (D) 15 mM. The HRT was fixed at 0.42 min. The empty symbols represent experimental data, and the error bars indicate standard deviations of triplicate experiments. The solid lines are generated using the DSS MCDI model and not from statistically fitting the experimental data. We note that Figure 4C presents a subset of data presented in Figure 3B.

Na^+ is controlled kinetically, not by equilibrium distribution as described by electrical double layer theory. In this case, the ratio between the two ion fluxes ($N_{Ca^{2+}}/N_{Na^+}$), which is proportional to the ratio of ion removal in the charging step, can be expressed using the following equation:

$$\frac{N_{Ca^{2+}}}{N_{Na^+}} = \frac{2D_{Ca^{2+}}c_{sp,Ca^{2+}}}{D_{Na^+}c_{sp,Na^+}} \quad (6)$$

In an aqueous solution, the diffusion coefficient of Na^+ is roughly twice that of Ca^{2+} (1.33×10^{-9} m^2 s^{-1} vs 0.79×10^{-9} m^2 s^{-1}).[24] Therefore, the two ions have similar electrical mobilities, as the difference between their diffusion coefficients is offset by the difference in ionic charges. Therefore, in the absence of CEM, the ionic flux ratio should be roughly proportional to the ratio between Ca^{2+} and Na^+ concentrations. In other words, there should not be any apparent preference of removing Ca^{2+} over Na^+ in CDI without integration of CEM in a dynamic adsorption process (e.g., constant current charging). The absence of such selectivity has indeed been confirmed by experiments showing that $N_{Ca^{2+}}/N_{Na^+}$ is proportional to $c_{sp,Ca^{2+}}/c_{sp,Na^+}$ ("+" in Figure 5). Because the ratio of removal equals the ratio of fluxes, which in this case also equals the ratio of aqueous concentrations between the two cationic species, removing ions from the feed solution does not change the ratio of aqueous concentrations. Therefore, $c_{sp,Ca^{2+}}/c_{sp,Na^+}$ is equal to $c_{0,Ca^{2+}}/c_{0,Na^+}$ in the absence of CEM.

The presence of CEM changes the electrical mobility of both Ca^{2+} and Na^+ ions and renders them very different. Because typical CEMs have a $P_{Na^+}^{Ca^{2+}}$ (defined in eq 5) from 2.4 to 4.5,[25] they facilitate faster transport of Ca^{2+} over Na^+. Combining eqs 4 and 5 reveals a linear relationship between the ratio of ion fluxes through the CEM, $(N_{Ca^{2+}}/N_{Na^+})_m$, and the ratio of concentrations in the spacer channel, $c_{sp,Ca^{2+}}/c_{sp,Na^+}$. Because ion transport through the CEM is the rate-limiting step (diffusion coefficients of Ca^{2+} and Na^+ in the aqueous phase are at least an order of magnitude higher than that in the CEM phase[23,24]), the overall ion flux ratio, $N_{Ca^{2+}}/N_{Na^+}$, should be approximately equal to the ion flux ratio in the CEM, $(N_{Ca^{2+}}/N_{Na^+})_m$, which is in turn proportional to $c_{sp,Ca^{2+}}/c_{sp,Na^+}$. This is indeed confirmed by the observed linear relationship between $N_{Ca^{2+}}/N_{Na^+}$ and $c_{sp,Ca^{2+}}/c_{sp,Na^+}$ (Figure 5). Such a linear relationship holds regardless of the feed composition and HRT, at least within the range of the investigated concentrations, which was confirmed by multiple series of experiments (Figure 5). All data points virtually collapse into one straight line that has a slope of 3.48. This suggests that the CEM used has a $P_{Na^+}^{Ca^{2+}}$ of 3.48 according to eq 4. We note that the linear scaling may not necessarily hold over a much larger range of feed concentrations, as the concentration dependence of the partition coefficients (K_{Na^+} and $K_{Ca^{2+}}$) may change the $K_{Ca^{2+}}/K_{Na^+}$ ratio that is required to be constant for the linear relationship in Figure 5 to hold. We also note that the linear scaling applies to only kinetically controlled ion transport (e.g., MCDI with a constant current) but not for ion transport near thermodynamic equilibrium as observed in a prolonged constant-voltage charging process.[22]

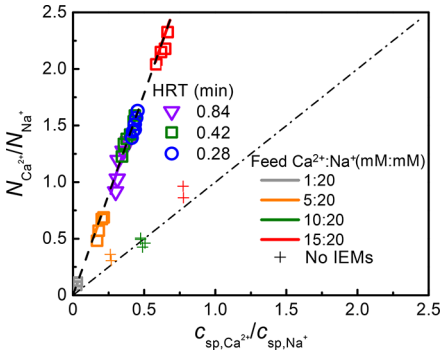

Figure 5. Ratio between fluxes of Ca^{2+} and Na^+ ($N_{Ca^{2+}}/N_{Na^+}$) as a function of ratio between spacer channel concentrations of Ca^{2+} and Na^+ ($c_{sp,Ca^{2+}}/c_{sp,Na^+}$) for both MCDI (colored symbols and dashed line) and CDI without IEM (black crosses and dotted−dashed line). The data from MCDI experiments were obtained using different HRTs and current densities (with a fixed feed composition) or using different feed compositions and current densities (with a fixed HRT). Different colors correspond to different feed compositions, while different symbol shapes represent different HRTs. The dashed line was obtained by fitting the MCDI and the CDI data using linear regression, respectively. The colored solid segments falling on the dashed line were simulated with the DSS MCDI model. The dotted−dashed line with a slope of unity represents a selectivity of 1.

Factors That Affect Selectivity. The selectivity of Ca^{2+} over Na^+, $\rho(Ca^{2+}/Na^+)$, with the definition based on eq 1, depends on current density, HRT, and feed composition. In general, $\rho(Ca^{2+}/Na^+)$ decreases with an increase in current density and HRT (Figure 6A). An increasing current density and an increasing HRT both result in more ion reduction and thus lower the spacer channel concentrations for both Ca^{2+} and Na^+ ions. According to the definition of $\rho(Ca^{2+}/Na^+)$, if

DOI: 10.1021/acs.est.9b00655
Environ. Sci. Technol. 2019, 53, 5797−5804

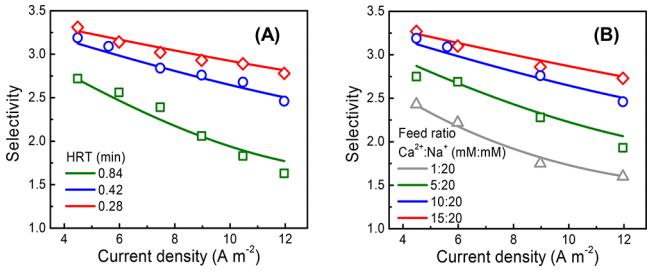

Figure 6. (A) Selectivity as a function of current density with different HRTs. (B) Selectivity as a function of current density with different feed compositions. The empty symbols are calculated from experimental data. The solid lines are simulated using the DSS MCDI model.

the feed concentrations $c_{0,Ca^{2+}}$ and $c_{0,Na^{+}}$ are fixed, $\rho(Ca^{2+}/Na^{+})$ is dependent on $\Delta c_{Ca^{2+}}/\Delta c_{Na^{+}}$. Because $\Delta c_{Ca^{2+}}/\Delta c_{Na^{+}}$ is proportional to $N_{Ca^{2+}}/N_{Na^{+}}$, it strongly depends on the ratio of spacer channel concentrations, $c_{sp,Ca^{2+}}/c_{sp,Na^{+}}$, according to eq 6. If $c_{0,Na^{+}}$ is significantly higher than $c_{0,Ca^{2+}}$, $c_{sp,Ca^{2+}}$ is much more sensitive than $c_{sp,Na^{+}}$ to the removal of the respective ions by a similar magnitude. Therefore, a higher degree of ion removal generally results in a lower $c_{sp,Ca^{2+}}/c_{sp,Na^{+}}$ ratio, which in turn reduces $N_{Ca^{2+}}/N_{Na^{+}}$ (based on eq 6) and thus the selectivity. This explains the dependence of selectivity on the current density and HRT, because a higher current density and a lower HRT both contribute to more salt removal and thus a lower $c_{sp,Ca^{2+}}/c_{sp,Na^{+}}$.

A higher Ca^{2+} concentration in the feed solution has two major impacts on selectivity, $\rho(Ca^{2+}/Na^{+})$. On the one hand, the increase in the $c_{0,Ca^{2+}}/c_{0,Na^{+}}$ ratio tends to reduce the selectivity based on the definition of selectivity given by eq 1. On the other hand, the increase in $c_{0,Ca^{2+}}/c_{0,Na^{+}}$ leads to an increase in $c_{sp,Ca^{2+}}/c_{sp,Na^{+}}$, which in turn causes a higher $\Delta c_{Ca^{2+}}/\Delta c_{Na^{+}}$ and tends to increase selectivity. Both the experimental results and theoretical simulation suggest that the second effect outcompetes the first effect regardless of current density (Figure 6B) and that a higher $c_{0,Ca^{2+}}/c_{0,Na^{+}}$ consistently leads to a higher selectivity, provided the Na^{+} concentration is kept the same. Lastly, we note that the 0D DSS MCDI model, though developed with certain simplifying assumptions, is sufficiently effective in predicting the selectivity of an MCDI process under different conditions, as evidenced by the remarkable agreement between the experimental data and the model simulations shown in Figure 6.

Trade-Off among Selectivity, Calcium Removal, and Calcium Removal Rate. If we increase the current density while fixing the HRT, the ion removal rates (i.e., ASAR) increase for both Ca^{2+} and Na^{+} ions, which is not surprising because a higher current density enhances the desalination rate. If we focus on the removal of Ca^{2+} as what is intended to be removed by softening, we observe a clear trade-off between selectivity and $ASAR_{Ca^{2+}}$ for a given HRT (Figure 7A). Both experimental results and numerical simulations suggest that selectivity decreases with an increase in $ASAR_{Ca^{2+}}$, following a virtually negative linear relationship.

The decrease in Ca^{2+} concentration, $\Delta c_{Ca^{2+}}$, is proportional to the product of $ASAR_{Ca^{2+}}$ and HRT, which allows us to collapse the three sets of data on Figure 7A into a single set of data in Figure 7B that plots selectivity versus $\Delta c_{Ca^{2+}}$.

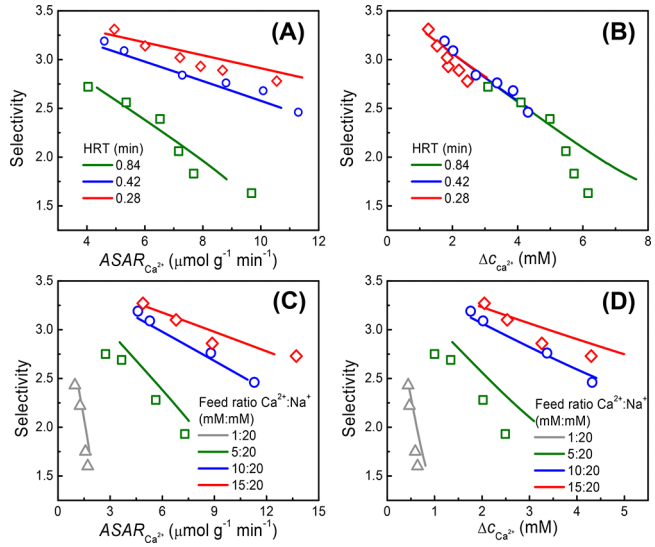

Figure 7. (A) Selectivity as a function of $ASAR_{Ca^{2+}}$ with different HRTs. (B) Selectivity as a function of $\Delta c_{Ca^{2+}}$ with different HRTs. (C) Selectivity as a function of $ASAR_{Ca^{2+}}$ with different feed compositions. (D) Selectivity as a function of $\Delta c_{Ca^{2+}}$ with different feed compositions. The empty symbols are calculated from experimental data. The solid lines are simulated using the 0D DSS MCDI model.

Interestingly, for a given feed composition, selectivity is a simply a function of $\Delta c_{Ca^{2+}}$ regardless how such a $\Delta c_{Ca^{2+}}$ is achieved. In other words, it does not matter if a certain $\Delta c_{Ca^{2+}}$ is achieved with a combination of a high current density and a short HRT or a combination of a low current density and a long HRT; the same $\Delta c_{Ca^{2+}}$ leads to the same selectivity. The negative correlation between selectivity and $\Delta c_{Ca^{2+}}$ as shown by Figure 7B implies that removing more Ca^{2+} from a feed solution of fixed composition using an MCDI process sacrifices the selectivity.

Selectivity also has a similar negative linear correlation with $ASAR_{Ca^{2+}}$ when the HRT is fixed but the feed composition changes (Figure 7C). Increasing $c_{0,Ca^{2+}}$ while maintaining $c_{0,Na^{+}}$ enhances the selectivity in general, as a higher $c_{0,Ca^{2+}}/c_{0,Na^{+}}$ also leads to a higher $c_{sp,Ca^{2+}}/c_{sp,Na^{+}}$ that is beneficial to the preferential removal of Ca^{2+}. In addition, selectivity is more sensitive to the change in $ASAR_{Ca^{2+}}$ when $c_{0,Ca^{2+}}/c_{0,Na^{+}}$ is low. For example, when $c_{0,Ca^{2+}}$ and $c_{0,Na^{+}}$ are 1 and 20 mM, respectively, selectivity sharply declines with just a slight increase in $ASAR_{Ca^{2+}}$. The different sensitivity of selectivity to the change in $ASAR_{Ca^{2+}}$ can be explained by the fact that selectivity is proportional to $c_{sp,Ca^{2+}}/c_{sp,Na^{+}}$ and that the percentage change in $c_{sp,Ca^{2+}}$ caused by a given increase in $ASAR_{Ca^{2+}}$ is much more dramatic when the initial concentration, $c_{0,Ca^{2+}}$, is low. Converting $ASAR_{Ca^{2+}}$ in Figure 7C to $\Delta c_{Ca^{2+}}$ in Figure 7D does not collapse the trade-off curves or result in any considerable change in the relative positions between these trade-off curves. This is because the HRT involved in such a conversion is identical for all trade-off curves in Figure 7C.

Similar Trade-Off Relationship Observed in Flow-Electrode CDI. The analysis on MCDI described above is performed mainly on the basis of ion transport kinetics across

DOI: 10.1021/acs.est.9b00655
Environ. Sci. Technol. 2019, 53, 5797−5804

the CEM and does not involve the specific mechanism of adsorption of the ion to the film carbon electrode. Therefore, it should be expected that similar conclusions from the analysis presented above also apply to flow-electrode CDI (FCDI) that employs IEMs. To show the universality of these conclusions, we analyze a set of data from a recent FCDI study reported by He et al.[26] The same negative linear correlation between selectivity and $ASAR_{Ca^{2+}}$ observed in MCDI (Figure 7A) is also in FCDI (Figure 8A). The major difference is that

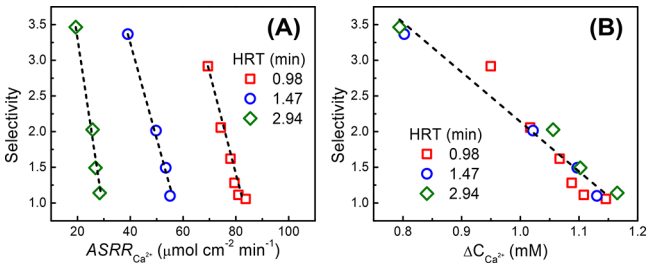

Figure 8. Analysis using literature data (ref 26) where flow-electrode CDI (FCDI) was employed to selectively remove Ca^{2+} from a brackish water containing both Ca^{2+} and Na^{+}: trade-offs between selectivity and (A) $ASRR_{Ca^{2+}}$ and (B) $\Delta c_{Ca^{2+}}$ with different HRTs. In FCDI, ion removal occurs as a combination of electrodialysis and electrosorption, and average salt removal rate (ASRR) is used instead of ASAR as in CDI. Conventionally, ASRR is the mass of ion removed normalized by the effective area between the flow electrode and the IEM. Empty symbols in the figure are experimental data extracted from ref 26, and the black dashed lines are drawn to guide eyes.

selectivity is significantly more sensitive to the average salt removal rate for Ca^{2+}, $ASRR_{Ca^{2+}}$ (equivalent to $ASAR_{Ca^{2+}}$ in MCDI) resulting from an increased current density in FCDI than in MCDI for a given HRT. This implies that it may be a better strategy to operate FCDI with a relatively low current density as the sacrifice in $ASRR_{Ca^{2+}}$ is insignificant but the improvement in selectivity is dramatic. If a high $ASRR_{Ca^{2+}}$ needs to be achieved, it can be achieved without sacrificing selectivity by reducing the HRT while maintaining a low current density.

Collapsing the three trade-off lines in Figure 8A by plotting selectivity against $\Delta c_{Ca^{2+}}$ again shows an inherent linear trade-off between selectivity and $\Delta c_{Ca^{2+}}$ in FCDI (Figure 8B), which is similar to what has been observed with MCDI as shown in Figure 7B. This suggests that, as long as the feed composition is the same, selectivity is simply a function of the amount of Ca^{2+} removed during the FCDI process. Removing more Ca^{2+} must be achieved at the cost of lower selectivity, regardless of how the higher $\Delta c_{Ca^{2+}}$ is attained. These very similar behaviors between MCDI and FCDI clearly suggest that it is the ion transport through CEM, not the specific mechanism of ion adsorption onto activated carbon, that determines the performance of selective ion removal during the CDI process.

IMPLICATIONS

The presence of trade-off relations between selectivity and $ASAR_{Ca^{2+}}$ and between selectivity and $\Delta c_{Ca^{2+}}$ has important practical implications for using MCDI for water softening, especially when considering the impacts of operating conditions on system performance (i.e., Figure 7A,B). To simplify our discussion, let us assume that the central objective of softening is to decrease the Ca^{2+} concentration and that decreasing the Na^{+} concentration is simply an unavoidable "side effect". In this case, the calcium-specific energy consumption, $SEC_{Ca^{2+}}$, which is the energy consumed to remove 1 mol of Ca^{2+}, can be employed as an important performance metric for energy efficiency.

For a given feed composition, we know that $SEC_{Ca^{2+}}$ increases if we attempt to achieve a higher $ASAR_{Ca^{2+}}$ or a higher $\Delta c_{Ca^{2+}}$. The former effect reflects the intrinsic trade-off between energy and kinetic efficiency, that it simply takes more energy to drive a faster MCDI process.[38] The second effect can be attributed to the fact that, as more ions are removed, the spacer channel ion concentrations decrease and the spacer channel resistance increases accordingly.[42,43] However, in both cases, there is an additional effect of increasing $ASAR_{Ca^{2+}}$ or $\Delta c_{Ca^{2+}}$ on $SEC_{Ca^{2+}}$, which is related to selectivity. The reduced selectivity with an increased $ASAR_{Ca^{2+}}$ or $\Delta c_{Ca^{2+}}$ demands that more Na^{+} ions be removed per Ca^{2+} ion removed, and therefore, more energy will be "waste" in removing the extra Na^{+}. This selectivity effect adds to the other effects mentioned above and renders either fast or "deep" softening using MCDI more energy intensive in terms of $SEC_{Ca^{2+}}$.

While this study is focused on selective removal of Ca^{2+} over Na^{+} as an example of water softening, the mechanistic insights revealed in this study should apply to all other selective ion removal processes using CDI with IEMs. Lastly, we also note that while integrating IEMs was originally proposed as a method to enhance the energy efficiency of CDI via increasing the charge efficiency by suppressing co-ion repulsion, the fact that IEMs promote preferential transport of certain ions over others makes CDI with IEMs effective for selective ion removal. This is true for MCDI, as demonstrated in this study, and for flow-electrode CDI, which also has to employ IEMs.

ASSOCIATED CONTENT

Supporting Information

The Supporting Information is available free of charge on the ACS Publications website at DOI: 10.1021/acs.est.9b00655.

Parameter settings for the ion transport model (Table S1), ion adsorption over the multiple repeating cycles (Table S2), schematic layout of one MCDI cell (Figure S1), removed charges as a function of current density with different feed compositions (Figure S2), and time series of cell voltage in an MCDI process with CC-ZV operation (Figure S3) (PDF)

AUTHOR INFORMATION

Corresponding Author

*E-mail: shihong.lin@vanderbilt.edu. Telephone: +1 (615) 322-7226.

ORCID

Li Wang: 0000-0002-5542-6696

Shihong Lin: 0000-0001-9832-9127

Notes

The authors declare no competing financial interest.

ACKNOWLEDGMENTS

The authors are grateful to the National Science Foundation for its support via Grant CBET-1739884.

DOI: 10.1021/acs.est.9b00655
Environ. Sci. Technol. 2019, 53, 5797−5804

REFERENCES

(1) Ahn, M. K.; Chilakala, R.; Han, C.; Thenepalli, T. Removal of Hardness from Water Samples by a Carbonation Process with a Closed Pressure Reactor. *Water* **2018**, *10* (1), 54.

(2) Osorio, V. K. L.; de Oliveira, W.; El Seoud, O. A.; Cotton, W.; Easdon, J. Hard Water and Soft Soap: Dependence of Soap Performance on Water Hardness. *J. Chem. Educ.* **2005**, *82* (2), 257.

(3) Koo, C. H.; Mohammad, A. W.; Fatihah, S. Recycling of oleochemical wastewater for boiler feed water using reverse osmosis membranes — A case study. *Desalination* **2011**, *271* (1−3), 178−186.

(4) Spellman, F. R. *Handbook of water and wastewater treatment plant operations*, 3rd ed.; CRC Press: Boca Raton, FL, 2013.

(5) Chao, P.; Westerhoff, P. Assessment and optimization of chemical and physicochemical softening processes. *J. - Am. Water Works Assoc.* **2002**, *94* (3), 109−119.

(6) Wachinski, A. M. *Ion exchange treatment for drinking water*; American Water Works Association: Denver, 2004.

(7) Pizzi, N. G. *Water treatment: Principles and practices of water supply operations series*, 4th ed.; American Water Works Association: Denver, 2010.

(8) Al Abdulgader, H.; Kochkodan, V.; Hilal, N. Hybrid ion exchange - Pressure driven membrane processes in water treatment: A review. *Sep. Purif. Technol.* **2013**, *116*, 253−264.

(9) Anderson, L.; Dicicco, J.; Sampson, H.; Wesley, D.; Walsh, M.-E.; Gagnon, G. A. Water Reclamation and Reuse. *Water Environ. Res.* **2014**, *86*, 1297−1313.

(10) Lee, H.-J.; Song, J.-H.; Moon, S.-H. Comparison of electrodialysis reversal (EDR) and electrode ionization reversal (EDIR) for water softening. *Desalination* **2013**, *314*, 43.

(11) Strathmann, H. Electrodialysis, a mature technology with a multitude of new applications. *Desalination* **2010**, *264* (3), 268−288.

(12) Singh, R. *Membrane technology and engineering for water purification: application, systems design and operation*, 2nd ed.; Butterworth-Heinemann: Kidlington, England, 2015.

(13) Labban, O.; Chong, T. H.; Lienhard, J. H. Design and modeling of novel low-pressure nanofiltration hollow fiber modules for water softening and desalination pretreatment. *Desalination* **2018**, *439*, 58−72.

(14) Van der Bruggen, B.; Vandecasteele, C. Removal of pollutants from surface water and groundwater by nanofiltration: overview of possible applications in the drinking water industry. *Environ. Pollut.* **2003**, *122* (3), 435−445.

(15) Seo, S.-J.; Jeon, H.; Lee, J. K.; Kim, G.-Y.; Park, D.; Nojima, H.; Lee, J.; Moon, S.-H. Investigation on removal of hardness ions by capacitive deionization (CDI) for water softening applications. *Water Res.* **2010**, *44* (7), 2267−2275.

(16) Yoon, H.; Lee, J.; Kim, S.-R.; Kang, J.; Kim, S.; Kim, C.; Yoon, J. Capacitive deionization with Ca-alginate coated-carbon electrode for hardness control. *Desalination* **2016**, *392*, 46−53.

(17) Mossad, M.; Zhang, W.; Zou, L. Using capacitive deionisation for inland brackish groundwater desalination in a remote location. *Desalination* **2013**, *308*, 154−160.

(18) Porada, S.; Zhao, R.; van der Wal, A.; Presser, V.; Biesheuvel, P. M. Review on the science and technology of water desalination by capacitive deionization. *Prog. Mater. Sci.* **2013**, *58* (8), 1388−1442.

(19) Suss, M. E.; Porada, S.; Sun, X.; Biesheuvel, P. M.; Yoon, J.; Presser, V. Water desalination via capacitive deionization: what is it and what can we expect from it? *Energy Environ. Sci.* **2015**, *8* (8), 2296−2319.

(20) Biesheuvel, P. M.; van Limpt, B.; van der Wal, A. Dynamic Adsorption/Desorption Process Model for Capacitive Deionization. *J. Phys. Chem. C* **2009**, *113* (14), 5636−5640.

(21) Biesheuvel, P. M.; Zhao, R.; Porada, S.; van Der Wal, A. Theory of membrane capacitive deionization including the effect of the electrode pore space. *J. Colloid Interface Sci.* **2011**, *360* (1), 239−248.

(22) Zhao, R.; van Soestbergen, M.; Rijnaarts, H. H. M.; van der Wal, A.; Bazant, M. Z.; Biesheuvel, P. M. Time-dependent ion selectivity in capacitive charging of porous electrodes. *J. Colloid Interface Sci.* **2012**, *384*, 38−44.

(23) Luo, T.; Abdu, S.; Wessling, M. Selectivity of ion exchange membranes: A review. *J. Membr. Sci.* **2018**, *555*, 429−454.

(24) Goswami, A.; Acharya, A.; Pandey, A. K. Study of self-diffusion of monovalent and divalent cations in nafion-117 ion-exchange membrane. *J. Phys. Chem. B* **2001**, *105* (38), 9196−9201.

(25) Sata, T.; Sata, T.; Yang, W. Studies on cation-exchange membranes having permselectivity between cations in electrodialysis. *J. Membr. Sci.* **2002**, *206* (1), 31−60.

(26) He, C.; Ma, J.; Zhang, C.; Song, J.; Waite, T. D. Short-Circuited Closed-Cycle Operation of Flow-Electrode CDI for Brackish Water Softening. *Environ. Sci. Technol.* **2018**, *52* (16), 9350−9360.

(27) Porada, S.; Weingarth, D.; Hamelers, H. V. M.; Bryjak, M.; Presser, V.; Biesheuvel, P. M. Carbon flow electrodes for continuous operation of capacitive deionization and capacitive mixing energy generation. *J. Mater. Chem. A* **2014**, *2* (24), 9313−9321.

(28) Jeon, S. I.; Yeo, J. G.; Yang, S.; Choi, J.; Kim, D. K. Ion storage and energy recovery of a flow-electrode capacitive deionization process. *J. Mater. Chem. A* **2014**, *2* (18), 6378−6383.

(29) Jeon, S. I.; Park, H. R.; Yeo, J. G.; Yang, S.; Cho, C. H.; Han, M. H.; Kim, D. K. Desalination via a new membrane capacitive deionization process utilizing flow-electrodes. *Energy Environ. Sci.* **2013**, *6* (5), 1471−1475.

(30) Ma, J.; He, C.; He, D.; Zhang, C.; Waite, T. D. Analysis of capacitive and electrodialytic contributions to water desalination by flow-electrode CDI. *Water Res.* **2018**, *144*, 296−303.

(31) Strathmann, H. *Ion-Exchange Membrane Separation Processes*; Elsevier Science: Amsterdam, 2004.

(32) Choi, J.-H.; Kang, H.-S. Scale Formation by Electrode Reactions in Capacitive Deionization and its Effects on Desalination Performance. *Kongop Hwahak* **2016**, *27* (1), 74.

(33) Choi, J. H.; Kim, B. T. Hardness removal in membrane capacitive deionization with a selective cation exchange membrane. *Desalin Water Treat* **2017**, *66*, 97−102.

(34) Xu, P.; Drewes, J. E.; Heil, D.; Wang, G. Treatment of brackish produced water using carbon aerogel-based capacitive deionization technology. *Water Res.* **2008**, *42* (10−11), 2605−2617.

(35) van Limpt, B.; van der Wal, A. Water and chemical savings in cooling towers by using membrane capacitive deionization. *Desalination* **2014**, *342*, 148−155.

(36) Choi, J.; Lee, H.; Hong, S. Capacitive deionization (CDI) integrated with monovalentcation selective membrane for producing divalent cation-rich solution. *Desalination* **2016**, *400*, 38−46.

(37) Hassanvand, A.; Chen, G. Q.; Webley, P. A.; Kentish, S. E. A comparison of multicomponent electrosorption in capacitive deionization and membrane capacitive deionization. *Water Res.* **2018**, *131*, 100−109.

(38) Wang, L.; Lin, S. H. Intrinsic tradeoff between kinetic and energetic efficiencies in membrane capacitive deionization. *Water Res.* **2018**, *129*, 394−401.

(39) Wang, L.; Lin, S. H. Membrane Capacitive Deionization with Constant Current vs Constant Voltage Charging: Which Is Better? *Environ. Sci. Technol.* **2018**, *52* (7), 4051−4060.

(40) Zuo, K.; Kim, J.; Jain, A.; Wang, T.; Verduzco, R.; Long, M.; Li, Q. Novel Composite Electrodes for Selective Removal of Sulfate by the Capacitive Deionization Process. *Environ. Sci. Technol.* **2018**, *52* (16), 9486.

(41) Kim, Y.-J.; Kim, J.-H.; Choi, J.-H. Selective removal of nitrate ions by controlling the applied current in membrane capacitive deionization (MCDI). *J. Membr. Sci.* **2013**, *429*, 52−57.

(42) Dykstra, J. E.; Zhao, R.; Biesheuvel, P. M.; van der Wal, A. Resistance identification and rational process design in Capacitive Deionization. *Water Res.* **2016**, *88*, 358−370.

(43) Dykstra, J. E.; Porada, S.; van der Wal, A.; Biesheuvel, P. M. Energy consumption in capacitive deionization - Constant current versus constant voltage operation. *Water Res.* **2018**, *143*, 367−375.

DOI: 10.1021/acs.est.9b00655
Environ. Sci. Technol. 2019, 53, 5797−5804